

Subscriber access provided by The Library | University of Bath

Article

Photocatalytic Activation and Reduction of CO to CH over Single Phase Nano CuSnS: A Combined Experimental and Theoretical Study

Neha Sharma, Tilak Das, Santosh Kumar, Reshma Bhosale, Mukul Kabir, and Satishchandra Ogale

ACS Appl. Energy Mater., Just Accepted Manuscript • DOI: 10.1021/acsaem.9b00813 • Publication Date (Web): 01 Jul 2019

Downloaded from pubs.acs.org on July 9, 2019

Just Accepted

"Just Accepted" manuscripts have been peer-reviewed and accepted for publication. They are posted online prior to technical editing, formatting for publication and author proofing. The American Chemical Society provides "Just Accepted" as a service to the research community to expedite the dissemination of scientific material as soon as possible after acceptance. "Just Accepted" manuscripts appear in full in PDF format accompanied by an HTML abstract. "Just Accepted" manuscripts have been fully peer reviewed, but should not be considered the official version of record. They are citable by the Digital Object Identifier (DOI®). "Just Accepted" is an optional service offered to authors. Therefore, the "Just Accepted" Web site may not include all articles that will be published in the journal. After a manuscript is technically edited and formatted, it will be removed from the "Just Accepted" Web site and published as an ASAP article. Note that technical editing may introduce minor changes to the manuscript text and/or graphics which could affect content, and all legal disclaimers and ethical guidelines that apply to the journal pertain. ACS cannot be held responsible for errors or consequences arising from the use of information contained in these "Just Accepted" manuscripts.

Photocatalytic Activation and Reduction of CO₂ to CH₄ over Single Phase Nano Cu₃SnS₄: A Combined Experimental and Theoretical Study

Neha Sharma,^{#,a} Tilak Das,^{#,a} Santosh Kumar,^b Reshma Bhosale*,^a Mukul Kabir ^a and Satishchandra Ogale*,^a

^aDepartment of Physics and Centre for Energy Science, Indian Institute of Science Education and Research (IISER), Pune, Dr. Homi Bhabha Road, Pune, 411008, India.

^bDepartment of Chemical Engineering, University of Bath, Claverton, Bath BA2 7AY, U.K.

KEYWORDS: Photocatalysis, CO₂ reduction, solar fuels, Cu₃SnS₄, Cu-Sn terminated surface.

ABSTRACT

In view of the ability to absorb visible light and high surface catalytic activity, metal sulfides are rapidly emerging as promising candidates for CO₂ photoreduction, scoring over the traditional oxide-based systems. However, their low conversion efficiencies due to serious radiative recombination issues and poor stability restrict their real-life applicability. Enhancing their performance by coupling with other semiconductor based photocatalysts or precious noble metals as co-catalysts makes the process cost intensive. Herein, we report a single-phase ternary sulfide-Cu₃SnS₄ (CTS) as a robust visible light photocatalyst for selective photoreduction of CO₂ to CH₄. It showed remarkable 80 % selectivity for CH₄ evolution with the rate of 14 µmol/g/hr, without addition of any co-catalyst or scavenger. The mechanistic pathway for catalytic activity is elucidated by DFT calculations and *in situ* ATR, which imply formaldehyde pathway of hydrocarbon production. The Cu-Sn termination of the surface is shown to be the key factor for competent CO₂ absorption and activation as confirmed from our X-ray spectroscopy measurements and first principle calculations. This study provides foundation and insights for the rational design of sulfide-based photocatalysts to produce renewable fuel.

1. INTRODUCTION

Over usage of fossil fuels to meet the ever-increasing electricity demand has led to excessive anthropogenic CO₂ emissions in the environment resulting in several harmful consequences; global warming being the most alarming amongst all. Inspired by the natural photosynthesis process by plants, CO₂ reduction using photon energy from the sun and an active photocatalyst is considered as an attractive approach in this context, as it produces storable renewable fuel, and at the same time, mitigates the greenhouse gas emission.^{1,2,3,4}

The foremost and fundamental step in photocatalytic CO₂ reduction is the absorption of CO₂ on the surface of a photocatalyst. Besides adsorption, CO₂ activation and further reduction to value-added products are also the other two crucial steps for the completion of photocatalytic reaction efficiently. However, CO₂ is a highly stable and chemically inert molecule with linear geometry. Thermodynamically stable CO₂ molecule requires large Gibbs free energy (~393.5 kJ/mol. at 298 K) for bending and breaking of the C-O bonds.^{5,6} More specifically, the reduction of CO₂ in the presence of H₂O into hydrocarbon fuel such as CH₄ and CH₃OH is a multistep multi-electron-proton-coupled uphill reaction with a higher positive change in the Gibbs free energy of 818.3 kJ/mol and 702.2 kJ/mol, respectively. This makes the CO₂ reduction a grand challenge to the researchers.^{5,7} To overcome the difficulties in this current scenario, detailed investigations of highly active and selective photocatalytic systems and their surfaces, combining experimental and theoretical insights, are extremely essential.

Since Inoue and co-workers⁸ reported their pioneering work on the photocatalytic CO_2 reduction over TiO_2 , many such class of materials like metal oxides $(ZnO_2^{9,10}\ TiO_2^{11,12}\ Ga_2O_3^{13,14})$, metal sulfides $(CdS_2^{8,15,16}\ Bi_2S_3^{17}\ ZnS_1^{18}\ Cu_2S_2^{19},\ SnS_2^{20,21})$, phosphides $(GaP)^8$, and Nitrides $(C_3N_4^{22,23})$ have been studied in this context. Among them, the most popular choice of a photocatalyst is TiO_2

due to its low cost, high stability and non-toxicity. However, its relatively wide band-gap (~3.1-3.3 eV) and UV responsive nature (forms only about 4% of solar spectrum) seriously restrict its solar conversion efficiency. 12 Among the visible light active photocatalysts reported so far, metalsulfides are considered as excellent candidates for their high optical absorption in the visible region of the solar spectrum because of their narrow band gap and high catalytic activity.²⁴ In particular, binary sulfide CdS is well studied as an effective visible light photocatalyst with a narrow band gap of 2.4 eV along with favorable conduction band positioning of CdS.8 However, several technical issues limit the photo-assisted redox activities of CdS such as aggregation of CdS nanoparticles resulting in decrease in the effective surface area, photo-instability and photocorrosion, and consequently high rate of electron hole pair recombination^{15,16}. Among the ternary sulfides very few materials have yet been studied such as CuInS₂ which showed selective CH₄ production at 2.5 µmol/g/hr after coupling with TiO₂.²⁵ Kudo et al ²⁶ demonstrated CuGaS₂ as an efficient photocatalyst with a series of sulfide materials coupled with RGO-TiO₂ delivering 0.25 µmol/g/hr of CO gas. Most of them are either coupled with semiconductor or co-catalyst such as Pt to boost the performance but the current state-of-art requires much more improvement in the performance features. Nevertheless, stand-alone (without scavenger/co-catalyst/noble metal coupling) ternary sulfides for photocatalytic CO₂ reduction are till date unexplored. Moreover, explicit understanding of pristine surface of photocatalyst and CO₂ interaction over the sulfide surface is also still lacking.²⁷

Herein, we report for the first time a single-phase ternary metal sulfide Cu₃SnS₄ (CTS) as a highly stable stand-alone visible light photocatalyst for CO₂ reduction into C1 hydrocarbons. Although CTS is explored for the applications of solar cell and dye/pollutant degradation, to the best of our knowledge there is no report on its application for photocatalytic CO₂ reduction.^{28–30} In the gas

phase, photocatalytic CO₂ reduction over our pristine CTS delivered CH₄ as a major product with 80% selectivity (without the addition of any co-catalyst or scavenger) at the rate of 14 μmol/g/hr. Apart from the excellent photocatalytic activity, CTS also displayed very good photostability for more than 17 hrs. Experimentally, CTS showed its thermodynamic viability to reduce CO₂ to C1 hydrocarbon due to appropriate alignment of energy levels with respect to reduction potentials of CO₂. Besides, our density functional theory (DFT) calculations reveals that CTS has an explicit Cu-Sn terminated (001) surface which is extremely competent to promote CO₂ absorption as well as deformation. Additionally, *in situ* ATR could elucidate the genesis of intermediate species and reaction mechanism in photocatalytic CO₂ reduction over CTS. Over all, our results highlight that bivalency of Copper i.e. Cu¹⁺ or Cu²⁺ on the CTS surface plays a very crucial role in the CH₄ production through formate intermediates following the formaldehyde pathway. As per our knowledge, this is the first report on ternary sulfide CTS (without a co-catalyst or scavenger) for CO₂ photo-reduction analyzed via combined experimental and theoretical approach.

2. EXPERIMENTAL SECTION

2.1. Material Synthesis

The Cu₃SnS₄ nanoparticles were synthesized as given in our earlier report.³¹ Briefly, the metal precursors, namely copper acetylacetonate and tin chloride were taken in certain molar ratio with excess of thioacetamide as the sulfur precursor. The reagents were taken in a three neck vessel with formamide as the solvent and were degassed under nitrogen for half an hour with constant stirring. Then, the mixture was heated to 170 °C at a rate of 10 °C/min and kept at that temperature for one hour. After completion, the reaction was quenched to room temperature. The nanoparticles were obtained by centrifuging and washing with ethanol several times. The NPs were dried at 80 °C overnight.

2.2. Characterization

Material Characterization: To confirm the crystal structure of CTS powder X-Ray diffraction (XRD) was done using Bruker D8-Advance X-ray Diffractometer (Germany) with Cu ka (wavelength = 1.5418 Å). The Raman study was performed using LABRAM HR 800 from Jobin Yvon Horiba. Morphology of CTS samples were studied by scanning electron microscopy (SEM) which was done using FEI Nova Nano 450 SEM. The High-resolution transmission electron (TEM) microscopy was performed with FEI, Tecnai F30, and FEG system with 300 kV. The Brunauer-Emmett- Teller (BET) adsorption measurements for surface area calculation were done using Quadrasorb automatic volumetric instrument. X-ray Photoelectron Spectroscopy (XPS) study was performed using a PHI 5000 Versa Probe II equipped with a mono-chromatic Al Ka (1486.6 eV), a X-ray source and a hemispherical analyzer. Valence band XPS was performed on a Kratos Axis HSi spectrometer with a monochromated Al Kα X-ray source operated at 90 W and magnetic charge neutral-izer. The Ultraviolet-Visible diffuse reflectance spectrum (UV-VIS DRS) was obtained by SHIMADZU UV-3600 plus UV-VIS-NIR spectrophotometer with integrating sphere attachment. In situ ATR Infrared spectra were recorded on a Thermo Nicolet FT-IR spectrometer, equipped with a liquid nitrogen cooled MCT (mercury cadmium telluride) detector and an external attachment for ATR-IR measurements. The ATR crystal for a gas flowthrough cell is made of ZnSe with 45° reflection crystal.

Electrochemical Measurements

Mott-Schottky plot was obtained by performing the measurements in three-electrode system using AUTOLAB PGSTAT 30 potentiostat. In three-electrode system, Ag/AgCl was used as reference electrode, Platinium as counter electrode, and sample coated on Fluorine doped Tin oxide (FTO) as the working electrode. The measurements were carried out in 0.5 M Na₂SO₃ electrolyte. The

photoelectrodes were fabricated by preparing the slurry in mortar pistil by adding 40 mg sample, 200 ul Nafion (5%) and 1ml iso-propanol (IPA). The obtained paste was coated on FTO with 1cm² area and heated at 250°C for 1hr to get homogenous film. Mott Schottky plots were recorded in dark at the scan rate of 10 mV/s with the frequency of 10 KHz. HER plots were obtained in a three electrode system with glassy carbon electrode (GCE) as the working electrode by using CH instruments.

Photocatalytic measurements

Gas phase photocatalytic CO₂ reduction experiments were carried out in a setup made of stainless-steel photoreactor with quartz window, under the illumination of solar simulator (100 mW/cm²) equipped with Xenon lamp. Prior to irradiation the reaction set up is vacuum treated, purged with He (20 ml/min for 1 hr) to remove the internal air and purged with high purity CO₂ for 1 hr along with water vapour. During irradiation 1ml of gaseous product from the setup is sampled and subsequent analysis was done by Gas Chromatography (Shimadzu Tracera GC-2010 Plus) with Barrier Ionization Detector (BID) and He carrier gas. Liquid products were also analysed periodically from separate aliquots on an Agilent 1260HPLC fitted with a Hi Plex column, however only traces of methanol detected in this study. For stability test, CTS sample was collected after each run, refreshed by washing with water and its performance was re-evaluated by the aforementioned procedure. The Selectivity of formed CO was deduced according to the following equation:

% of CH₄ selectivity =
$$\frac{8N_{CH4}}{8N_{CH4} + 2N_{CO} + 2N_{H2}} \times 100$$

In which, N_{CH4} , N_{CO} and N_{H2} stand for the yield of reactively formed CH_4 , CO and H_2 , respectively.

% of CO selectivity =
$$\frac{2N_{CO}}{8N_{CH4} + 2N_{CO} + 2N_{H2}} \times 100$$

In which, N_{CO} and N_{H2} stand for the yield of reactively formed CO and H₂, respectively.

Apparent quantum yield (AQY) of the photocatalyst was calculated using the following equation:

$$AQY \% = \frac{\text{The number of evolved CH4 molecules } \times 8}{\text{The number of incident photons}} \times 100$$

3. RESULTS AND DISCUSSION

Phase purity of the orthorhombic Cu₃SnS₄ nanoparticles was confirmed by X-ray diffraction (XRD) as reported earlier and is shown in Figure S14 (a).³¹ Morphological and microstructural features were also studied by FESEM and TEM techniques and the corresponding images are given in the Supporting Information Figure S14. These reveal that the size of CTS nanoparticles is about 5 nm. The positive slope in Mott-Schottky plot as given in the inset of **Figure 1a** indicates n-type conductivity of CTS. To evaluate the thermodynamic feasibility of CTS in the targeted application context, band levels were estimated from the band-gap and Valence Band (VB) spectroscopies. The Tauc plot (Supporting information S1) derived from the DRS depicts the optical band gap of 1.76 eV, implying CTS as a visible light photocatalyst. The measured VB edge of CTS (Figure 1a) is 0.64 eV. Hence, the CB (conduction band) for CTS from the band-gap is calculated to be -1.12 eV vs. NHE. Thus, with the obtained values for CB and VB of CTS, it is possible to derive a schematic energy level diagram with respect to reduction potentials of CO₂ to different reduced products as given in Figure 1b. It clearly indicates that in CTS the CB edge has much more negative potential relative to required reduction potential of CO₂ to get reduced products and it is indeed a thermodynamically viable visible light-driven photocatalyst. We also performed DFT calculations with Van der Waals dispersion energy corrections (at D3 level) 32,33 to study the surface of CTS.³¹ Since (001) is the preferred orientation obtained from the XRD, we have

performed all the DFT calculations on the same surface. It is demonstrated that (001) surface of CTS is Cu-Sn terminated with sublayer of S atom as shown in the schematic (**Figure 2b**).

Photocatalytic CO₂ Reduction over CTS (001) surface

Experimentally, after 5 hrs of gas phase photoreduction of CO_2 on CTS sample $CH_4 \sim (71 \mu mol/g)$, $CO \sim (42 \mu \text{mol/g})$ and $H_2 \sim (31 \mu \text{mol/g})$ were obtained as resultant reduced products, as shown in Figure 1c. Trace amount of CH₃OH was also detected by HPLC. O₂ evolution ~ (178 μmol/g) was the oxidised product from water oxidation reaction (discussed in details in Supporting Information S2 a). The total volume of the O₂ produced was correlated with the total volume of reduced products which indicate that (CO+H₂): O₂ and CH₄: O₂ ratio is in the stoichiometric ratio of 2:1 and 1:2, respectively, which indicates that water is consumed as a reducing agent (electron donor) in the overall reaction. The control experiment (Supporting Information S2 b) indicates that almost no CO or hydrocarbon is detected in the absence of either the photocatalyst or light, suggesting that the obtained reduced products are the result of the photocatalytic reaction on the surface of the photocatalyst. Secondly, in the absence of the CO₂ gas, no products were evolved indicating unequivocally that the carbon source of reduced products (CO and CH₄) is from CO₂ and not from any other source Among the obtained products, CH₄ was produced as a major product with 80% selectivity at the rate of 14 µmol/g/h without addition of any co-catalyst or scavenger agent. Moreover, reusability of CTS evaluated by successive 3 cyclic runs for 17 hrs of light illumination (**Figure 1d**) could be clearly established and signifies that CTS surface has very good stability for longer run experiments. The same is shown in the form of histograms with three repetitions for CH₄, CO and H₂ in Figure S15 of SI.

X-ray Photoelectron Spectroscopy (XPS) Analysis of CTS (001) Surface

The step of CO₂ adsorption is not only the necessity but also the foundation towards increasing the CO₂ uptake and photoactivity of a solid photocatalyst. To gain the insights into the exact mechanism and the role of Cu exposed CTS surface experimentally as well as theoretically, XPS data was analysed as given in **Figure 2**.

The Cu 2p spectrum display two peaks positioned at 2p_{3/2} (932.3 eV) and 2p_{1/2} (952.1 eV), which is deconvoluted into doublets. This indicates the presence of Cu¹⁺ and Cu²⁺ on the CTS NPs surface.^{34,35,36} The concentration of Cu¹⁺ on the surface of CTS is more as compared to Cu²⁺ which is in agreement with DFT prediction (details in Supporting Information S3). From our calculations using PBE-GGA functional of the core levels of Cu ions using the core-hole approach as implemented in Wien2K code³⁷ showed results for the L₂ edges of the two types of Cu atoms (~948 eV) indicating existence of copper in both Cu¹⁺ and Cu²⁺ on the surface of CTS in accordance with experimental interpretation from XPS. However, the exact stoichiometric amount of the Cu¹⁺ and Cu²⁺ in the slab cannot be predicted from the present ground state first-principles core-hole calculations. The details of experimentally measured Sn and S XPS results are given in Figure S3. Thus, the surface edge with Cu-Sn termination represents the most available active sites for the catalytic reactions, supported by sub-layer of S atoms in a pristine CTS (001) surface. Therefore, over the Cu-Sn terminated (001) surface of CTS interaction of CO₂ and H₂O molecules was studied by DFT+D3 level as to probe the mechanism of CO₂ reduction.

Mechanism of H₂O Breaking and CO₂ Activation from DFT Prediction

As the activation of the CO₂ molecule is highly assisted in the presence of water vapour under the present experimental conditions, adsorption process of the H₂O molecule over the CTS surface

was examined preliminarily from our first-principles DFT+D3 theoretical calculations (Supporting Information S4 and Table S1). Herein, we considered only three possibilities for H_2O adsorption due to the polar and more electronegative character of the H_2O , which can be a best fitted to the three available metal sites on the CTS surface. (Details are in Supporting Information S5). Out of these three types of metal sites, only Cu^{1+} or Cu^{2+} sites are highly favourable for the H_2O physisorption with calculated binding energies -0.2 eV whereas the Sn-site does not accept the H_2O due to positive binding energy. The measured <H-O-H> angle is ~106.5 after the optimization of the atomic positions using DFT+D3 level functional, which led to out-of-plane distances of ~0.227 and 0.224 nm from Cu^{1+} and Cu^{2+} sites of CTS (001) surface, respectively. Indeed, the calculated Fermi level is up-shifted due to H_2O adsorption at Cu sites by ~0.15 eV than the pure CTS surface from our calculations, which is also another signature of weak physisorption of H_2O over the CTS surface ($H_2O@CTS$).

Similarly, the calculated binding energies of the different possible models of the isolated CO_2 over the Sn-Cu terminated (001) surface of the CTS are shown in the Table S1 of SI. We note a clear indication that isolated CO_2 can be physisorbed as the values of E_b are within few tens to few hundreds of meV per mole. Out of all the models, the best preferred site for the CO_2 is the hollow site enclosed by Cu^{1+} - Cu^{2+} - Cu^{1+} triangle with linear CO_2 perpendicular to the Cu^{1+} - Cu^{1+} chain, with calculated binding energy of -0.660 eV per molecule of CO_2 (Supporting Information S6 in Model [b] and Table S1), followed by the three models i.e. i) model [a] with O-atom of CO_2 over the Cu^{1+} of the CTS and perpendicular to the Cu^{1+} - Cu^{1+} chain with binding energies -0.135 eV, and ii) model [f] the next model with CO_2 within the hollow hexagon formed by Cu^{1+} - Sn^{4+} - Cu^{2+} triangle unit and parallel to Cu^{1+} - Cu^{2+} chain with binding energies -0.115 eV, and finally iii) model [d] the model with the CO_2 is perpendicular to the Cu^{1+} - Cu^{2+} chain, with calculated binding

energies -0.107 eV. We observed that in all these four models, the optimized CO₂ molecule remained linear and no activation (bending) is observed with calculated angles of CO₂ i.e. <O-C-O> are 179.5, 179.7, 179.6, and 179.7, respectively.

The current state-of-art of solo CO₂ adsorption scenario changes dramatically, once we combine best preferred sites for both the molecules, CO₂ and H₂O, over the CTS NPs (001) surface during computer modelling. Thus, we have proceeded with total four possible models by combination of these previously mentioned four models of CO₂@CTS and two models of H₂O@CTS to validate the route of CO₂ reduction (Details are in Supporting Information S7 of SI). The first step of the CO₂ reduction is single proton and two electron transfer, as given in the following equation³⁸,

$$CO_2 + H^+ + 2e^- = HCOO^- \text{ at } E_0 = -0.49 \text{V vs. NHE.}$$
 (1)

Similar kind of phenomena is observed in one of our proposed four models combining the CO_2 and H_2O with CTS from first-principles calculations with optimized hybrid geometry shown in **Figure 3a**, where only the specific projection of the 2×2 super cell structure is shown for better visualization. It is clear from the figure that the combined model $CO_2@CTS$ with the $H_2O@CTS$ best suits complete distortion of the CO_2 into OH^- and $HCOO^-$ via bending of CO_2 with angle $\sim 123^\circ$ which is reasonable with the required CO_2 activation angle of $\sim 120^\circ$ -140. Both the Cu sites are preferred to the H_2O adsorption, but thermodynamically the Cu^{2+} site is helpful in breaking of H_2O due to unfilled d orbital i.e. $3d^9$ by trapping the photo generated electrons. Consequently, Cu (II) gets converted to Cu (I) and trapped electrons are utilized in radical formation. The formed Cu (I) could be reoxidised to Cu (II) by protons from the system as given in equation (2) and (3). Such a sequential reaction reduces the rate of electron hole recombination increasing the selectivity and yield of reduced products. 39

$$Cu (II) + e^{-} \rightarrow Cu (I)$$
 (2)

$$Cu (I) + H^{+} \rightarrow Cu (II)$$
(3)

Hence, the accessibility of valency switching of Cu at the CTS surface plays an important cyclic oxidation and reduction of H_2O , respectively with constant generation of protons which is the key necessity for continuation and completion of CO_2 reduction. Such changes in valency mediated via the presence of native defect sites cannot be excluded; indeed, affecting overall changes of the charge state of Sn sites from Sn^{4+} to Sn^{2+} . More number of Cu^{1+} sites, are helpful to separate the protons and their radicals from rapid recombination as a donor, whereas the Cu^{2+} as an acceptor enhances the format redox route.

In **Figure 3b**, we have sketched one schematic following our first-principles calculated optimized geometry of the CTS (001) slab combining with H_2O and CO_2 . This is in accordance with our XPS observation of the two types of Sn sites present on pristine CTS surface. Once protons are available at the Cu^{2+} site, in the presence of CO_2 and photon the formation of $HCOO^-$ is feasible on the CTS surface as we observed from our DFT+D3 optimized structure analysis. One of the bond lengths of C-O is slightly larger (1.29 Å) than the far most C-O bond length (1.24Å), with Cu^{2+} -O distance ~ 2.3 Å which are favourable conditions for the CO_2 activation; those have been fulfilled here. Hence, the possible pathway of CO_2 photoreduction over CTS proceeds through formaldehyde way. The other three possible models of combined with CO_2 @CTS and H_2O @CTS, respectively, remain a weak physisorption process and can be ruled out in this present discussion (Details are in Supporting Information S7). To confirm the formaldehyde pathway experimentally *in situ* ATR was conducted over CTS surface.

In situ ATR Analysis for the Mechanism of Photocatalytic CO₂ Reduction

To detect the intermediate products and to obtain further insights into the mechanism of photocatalytic CO₂ reduction over CTS, *in situ* ATR measurements were conducted (Results in

molecule.5

Figure 4). IR of CTS purged with CO₂ gas and water vapour was recorded in dark and under light illumination for 30 mins and later for 60 mins to study the reaction sequence by ATR. In photocatalytic CO₂ reduction, when light is incident on the photocatalyst, electron-hole pair is generated and the photogenerated carriers migrates to the surface. The photogenerated electrons from the CB of the photocatalyst along with protons from H₂O reduce CO₂, as the photocatalyst has much more negative potential than the reduction potential of CO₂; while the holes from VB of the photocatalyst does oxidation of water to produce O₂. The resultant reduced products finally get desorbed from the surface. In the dark, combination bands of molecular CO₂ around (3500-3700 cm⁻¹) and molecular H₂O (2900-3500 cm⁻¹) from purged CO₂ and H₂O are observed.⁴⁰ Apart from molecular gas small vibration peaks of asymmetric stretching of CO₂ (2150-2200 cm⁻¹) and bending vibrations of -OH groups (1630-1640 cm⁻¹) are observed, indicating the interaction of these gases with CTS surface even in dark. 40,41 More surprisingly, a weak peak at 1264 cm⁻¹ is observed indicating the presence of CO₂.41,42 Existence of CO₂ radical as an intermediate species during the photoreduction of CO₂ by capturing the electron from the conduction of catalyst is a controversial issue due to its thermodynamic barrier.⁵ Additionally, its rapid conversion into further intermediates and product makes its detection difficult. Even many theoretical and experimental research groups have verified the CO₂ species by different configuration. 41,42,43,44 In our case also we observed bending of CO₂ on the Cu-Sn terminated (001) surface of CTS by DFT+D3 computation of geometry (Figure 3a). CO₂ adsorbate has a bent configuration and lower barrier to accept electrons for further activation of CO₂ as compared to the linear free CO₂

After light illumination, appearance of two new distinct broad bands at around 1200-1400 cm⁻¹ and 1550-1650 cm⁻¹ were clearly seen. The mode at around 1660 cm⁻¹ is characteristic of bidentate

carbonate b-CO₃²⁻ which indicates that CO₂ molecule is bonded to CTS surface through its oxygen rather than by carbon,^{5,42} which is well corroborated with interpretation from our DFT (S2 in Supporting Information). The bands at 1460 and 1621 cm⁻¹ correspond to bicarbonate species HCO₃ which arises from the reaction of absorbed CO₂ and surface hydroxyls from dissociative H₂O molecule.⁴² Two sharp bands at around 2160 and 2200 cm⁻¹ represent the asymmetric vibrations of CO₂ or CO bonded with Cu (I) and Cu (II),respectively.^{45,46} The existence of Cu¹⁺ and Cu²⁺ on the surface of CTS is also confirmed experimentally (XPS) and theoretically (DFT) in our case which is in agreement with the ATR results. Such bands indicate that the Cu terminated surface has important role to play for providing absorption site for CO₂ and for its deformation. Importantly, a new and broad band at around 1360 cm⁻¹ is observed which is attributed to asymmetric stretching of OCO arising from bidentate HCOO*. Formation of this species indicates that the photocatalytic mechanism may have proceeded through formaldehyde pathway by formation of bidentate formate as an intermediate species which finally leads to CH₄.^{42,47,48}

$$CO_2 \rightarrow HCOOH \rightarrow H_2CO \rightarrow CH_3OH \rightarrow CH_4$$
 (4)

Thermodynamically this is possible in the CTS case, as it has negative conduction band (-1.1 V vs NHE) compared to the reduction potential of CO₂ to HCOOH (-0.61V vs NHE) by transfer of two electrons.⁵ We also observed trace amount of methanol as a reduced product under the gas phase of experimental conditions, which perhaps must have got consumed further for the formation of CH₄ as per the equation (4). In addition, formate can reoxidize itself to produce CO. The very weak bands at around 1112 cm⁻¹ and 3019 cm⁻¹ are characteristics peaks of CO and CH₄, respectively ^{48,49}, which are an indication that formation of target products is initiated after the 30 mins of light illumination by the reaction of intermediate photoactive species: b-CO₃², HCO₃⁻, OCO, OH- by H₂ as reductant. Further, 60 mins of illumination showed increase in the peak

intensity of CO and CH₄ with subsequent reduction of b-CO₃²⁻, HCO₃⁻, OCO. Also, generation of a new distinct peak corresponding to C-H bending from C1 hydrocarbons is also observed at 1390 cm⁻¹.^{49,50} Combining our results based on the spectral changes it can be speculated that CO^{*}₂ and OCO are deemed to be the key intermediates for formation of bidentate formate which is utilized for the production of CH₄. Based on ATR results and formed products the possible mechanism can be elucidated by following equations:^{5,42,48,51,52}

$$CTS + h\nu = CTS (h^{+}_{VB} + e^{-}_{CB})$$

$$2H_2O + 4h^+ = 4H^+ + O_2$$
 (E⁰ = + 0.82 V)

$$CO_2 + e^- = CO_2$$
 (E⁰ = -1.90 V)

$$CO_2 + 2H^+ + 2e^- = CO + H_2O$$
 (E⁰ = -0.53 V)

$$CO_2 + 4OH^- = CO_3^{2-} + 2H_2$$

$$CO_3^{2-} + OH^- = HCO_3^- + 2O_2$$

$$CO_2 + 2H^+ + 2e^- = HCOOH$$
 (E⁰ = -0.61V)

$$CO_2 + 8H^+ + 8e^- = CH_4 + 2H_2O$$
 (E⁰ = -0.24 V)

$$CO_2 + 6H^+ + 6e^- = CH_3OH + H_2O \quad (E^0 = -0.38 \text{ V})$$

$$2H^+ + 2e^- = H_2$$
 (E⁰ = -0.41 V)

Still the question remains as to how and why eight electrons and eight protons coupled process of particular CH₄ production is so favoured over the Cu-Sn surface as compared to other resultant reduced products of photo-reduction of CO₂. Firstly, Cu ions can act as an active centre for CO₂ photoreduction as they can trap the photo-generated electrons from the CTS surface due to unfilled

d-orbital, thereby inhibiting electron hole recombination. 42,45,46 Consequently, more number of photo generated electrons are available for activation of CO₂ and for the genesis of intermediate products, and ultimately should increase the quantum yield of photocatalyst. In our case as well, the obtained Apparent Quantum Yield (AQY) for CTS is 1.63% which is higher than the earlier reported values.^{53,54,55,56} Secondly, Cu not only participates in the activation of CO₂ but it also suppresses the simultaneously occurring undesirable HER reaction which ultimately increases CH₄ selectivity and yield as accumulated charges on the surface is well utilized in CO₂ reduction.^{57,58} To confirm the above, we also performed the electrochemical experiment to evaluate the HER activity of CTS in the presence of Ar and CO₂ both as given in Supporting Information S8 which clearly indicates that the Cu terminated CTS surface has more affinity for CO coverage, which weakens the binding of hydrogen on surface to produce H2. It is difficult to compare the CO2 reduction yield of products over CTS with other sulfides due to different experimental conditions but we have given a Table S2 of the comparison (Supporting information) where CTS stands at the top without any addition of co-catalyst of scavenger. In conclusion, Cu ion increases the probability of electrons transfer to adsorbed CO₂ and for the genesis of intermediate reactive species like CO₂ formate HCOO, which eventually forms C1 or higher hydrocarbons. The formation of CH₄ from the formaldehyde pathway proceeds through the formation of formate,

Conclusion

which is stabililized by the valence of Cu.

The present work demonstrates that single-phase ternary sulphide Cu₃SnS₄ nano-particulates as an efficient visible light photocatalyst for selective CO₂ reduction to CH₄. It shows an excellent photocatalytic performance of 71µmol/g of CH₄ with good selectivity and stability. We attempted to elucidate the mechanism by investigating and studying the pristine surface of CTS and

interaction of CO₂ over it. Our DFT+D3 predictions indicate that CTS possesses Cu-Sn terminated (001) surface which promotes CO₂ adsorption and activation. To summarize, from our experimental and theoretical calculations we conclude that Cu-Sn terminated CTS follows formaldehyde pathway for production of C1 hydrocarbon. The present work provides the foundation for the rational design of sulfide based photocatalyst to produce renewable fuel.

ASSOCIATED CONTENT

Supporting Information: Tauc plot, control experiment of photocatalytic CO_2 reduction, O_2 evolution data. Detail theoretical study of interaction of CO_2 and water vapour over CTS by DFT, HER plot and table of comparison of different catalyst with CTS.

AUTHOR INFORMATION

*Corresponding Authors

E-mail: reshmabhosale10@gmail.com

E-mail: satishogale@gmail.com, satishogale@iiserpune.ac.in

Author Contributions

The manuscript was written through contributions of all authors. All authors approve the final version of the manuscript. # Neha Sharma and # Tilak Das have contributed equally.

Notes

Authors declare no competing financial interest.

ACKNOWLEDGEMENT

Authors would like to thank DST Nanomission (Thematic Unit SR/NM/TP-13/2016), Govt. of India and the UK-India SUNRISE (GCRF) Grant for research funding. SK also thanks the

Engineering and Physical Sciences Research Council (EPSRC) (EP/R035407/1) for financial support. SO would like to thank the Department of Atomic Energy for the award of the Raja Ramanna Fellowship.

ABBREVIATIONS

CTS, Cu₃SnS₄; ATR, Attenuated Total Reflection; HER, Hydrogen Evolution Reaction.

REFERECES

- (1) White, J. L.; Baruch, M. F.; Pander, J. E.; Hu, Y.; Fortmeyer, I. C.; Park, J. E.; Zhang, T.; Liao, K.; Gu, J.; Yan, Y.; Shaw T. W.; Abelev E.; Bocarsly A. B. Light-Driven Heterogeneous Reduction of Carbon Dioxide: Photocatalysts and Photoelectrodes. *Chem. Rev.* 2015, 115 (23), 12888–12935.
- (2) Marszewski, M.; Cao, S.; Yu, J.; Jaroniec, M. Semiconductor-Based Photocatalytic CO₂ Conversion. *Mater. Horizons* **2015**, *2* (3), 261–278.
- (3) Di, T.; Xu, Q.; Ho, W. K.; Tang, H.; Xiang, Q.; Yu, J. Review on Metal Sulphide-Based Z-Scheme Photocatalysts. *ChemCatChem*. 2019, pp 1394–1411.
- (4) Li, X.; Yu, J.; Jaroniec, M.; Chen, X. Cocatalysts for Selective Photoreduction of CO₂ into Solar Fuels. *Chem. Rev.* **2019**, *119* (6), 3962–4179.
- (5) Chang, X.; Wang, T.; Gong, J. CO₂ Photo-Reduction: Insights into CO₂ Activation and Reaction on Surfaces of Photocatalysts. *Energy Environ. Sci.* **2016**, *9* (7), 2177–2196.
- (6) Álvarez, A.; Borges, M.; Corral-Pérez, J. J.; Olcina, J. G.; Hu, L.; Cornu, D.; Huang, R.; Stoian, D.; Urakawa, A. CO₂ Activation over Catalytic Surfaces. *ChemPhysChem* 2017, 18 (22), 3135–3141.

- (7) Kamat, P. V. Semiconductor Surface Chemistry as Holy Grail in Photocatalysis and Photovoltaics. *Acc. Chem. Res.* **2017**, *50* (3), 527–531.
- (8) Inoue, T.; Fujishima, A.; Konishi, S.; Honda, K. Photoelectrocatalytic Reduction of Carbon Dioxide in Aqueous Suspensions of Semiconductor Powders. *Nature*. 1979, pp 637–638.
- (9) Liu, X.; Ye, L.; Liu, S.; Li, Y.; Ji, X. Photocatalytic Reduction of CO₂ by ZnO Micro/Nanomaterials with Different Morphologies and Ratios of {0001} Facets. *Sci. Rep.* 2016, 6, 1–9.
- (10) Xin, C.; Hu, M.; Wang, K.; Wang, X. Significant Enhancement of Photocatalytic Reduction of CO₂ with H₂O over ZnO by the Formation of Basic Zinc Carbonate. *Langmuir* **2017**, *33* (27), 6667–6676.
- (11) Li, K.; Peng, B.; Peng, T. Recent Advances in Heterogeneous Photocatalytic CO₂
 Conversion to Solar Fuels. *ACS Catal.* **2016**, *6* (11), 7485–7527.
- Shehzad, N.; Tahir, M.; Johari, K.; Murugesan, T.; Hussain, M. A Critical Review on TiO₂
 Based Photocatalytic CO₂ Reduction System: Strategies to Improve Efficiency. *J. CO₂ Util.* 2018, 26 (November 2017), 98–122.
- (13) Park, H. A.; Choi, J. H.; Choi, K. M.; Lee, D. K.; Kang, J. K. Highly Porous Gallium Oxide with a High CO₂ Affinity for the Photocatalytic Conversion of Carbon Dioxide into Methane. *J. Mater. Chem.* **2012**, *22* (12), 5304–5307.
- Pan, Y. X.; Liu, C. J.; Mei, D.; Ge, Q. Effects of Hydration and Oxygen Vacancy on CO₂
 Adsorption and Activation on β-Ga₂O₃(100). *Langmuir* 2010, 26 (8), 5551–5558.
- (15) Yu, J.; Jin, J.; Cheng, B.; Jaroniec, M. A Noble Metal-Free Reduced Graphene Oxide-CdS Nanorod Composite for the Enhanced Visible-Light Photocatalytic Reduction of CO₂ to Solar Fuel. *J. Mater. Chem. A* **2014**, *2* (10), 3407–3416.

- (16) Li, Q.; Guo, B.; Yu, J.; Ran, J.; Zhang, B.; Yan, H.; Gong, J. R. Highly Efficient Visible-Light-Driven Photocatalytic Hydrogen Production of CdS-Cluster-Decorated Graphene Nanosheets. J. Am. Chem. Soc. 2011, 133 (28), 10878–10884.
- (17) Jin, J.; He, T. Facile Synthesis of Bi2S3 Nanoribbons for Photocatalytic Reduction of CO₂ into CH₃OH. *Appl. Surf. Sci.* **2017**, *394*, 364–370.
- (18) Zhou, R.; Guzman, M. I. CO₂ Reduction under Periodic Illumination of ZnS. *J. Phys. Chem.*C 2014, 118 (22), 11649–11656.
- Manzi, A.; Simon, T.; Sonnleitner, C.; Döblinger, M.; Wyrwich, R.; Stern, O.; Stolarczyk,
 J. K.; Feldmann, J. Light-Induced Cation Exchange for Copper Sulfide Based CO₂
 Reduction. J. Am. Chem. Soc. 2015, 137 (44), 14007–14010.
- (20) Sun, Y.; Li, G.; Xu, J.; Sun, Z. Visible-Light Photocatalytic Reduction of Carbon Dioxide over SnS₂. *Mater. Lett.* **2016**, *174*, 238–241.
- (21) Jiao, X.; Li, X.; Jin, X.; Sun, Y.; Xu, J.; Liang, L.; Ju, H.; Zhu, J.; Pan, Y.; Yan, W.; Lin Y.; Xie Y. Partially Oxidized SnS₂ Atomic Layers Achieving Efficient Visible-Light-Driven CO₂ Reduction. *J. Am. Chem. Soc.* 2017, 139 (49), 18044–18051.
- (22) Zhu, J.; Xiao, P.; Li, H.; Carabineiro, S. A. C. Graphitic Carbon Nitride: Synthesis, Properties, and Applications in Catalysis. ACS Appl. Mater. Interfaces 2014, 6, 16449– 16465.
- (23) Larmier, K.; Liao, W.-C.; Tada, S.; Lam, E.; Verel, R.; Bansode, A.; Urakawa, A.; Comas-Vives, A.; Copéret, C. CO₂-to-Methanol Hydrogenation on Zirconia-Supported Copper Nanoparticles: Reaction Intermediates and the Role of the Metal-Support Interface. *Angew. Chemie Int. Ed.* 2017, 56 (9), 2318–2323.
- (24) Navalón, S.; Dhakshinamoorthy, A.; Álvaro, M.; Garcia, H. Photocatalytic CO₂ Reduction

- Using Non-Itanium Metal Oxides and Sulfides. ChemSusChem 2013, 6 (4), 562–577.
- (25) Xu, F.; Zhang, J.; Zhu, B.; Yu, J.; Xu, J. CuInS₂ Sensitized TiO₂ Hybrid Nanofibers for Improved Photocatalytic CO₂ Reduction. *Appl. Catal. B Environ.* **2018**, *230* (2010), 194–202.
- (26) Takayama, T.; Sato, K.; Fujimura, T.; Kojima, Y.; Iwase, A.; Kudo, A. Photocatalytic CO₂ Reduction Using Water as an Electron Donor by a Powdered Z-Scheme System Consisting of Metal Sulfide and an RGO–TiO₂ Composite. *Faraday Discuss.* **2017**, *198*, 397–407.
- (27) Kamat, P. V.; Jin, S. Semiconductor Photocatalysis: "Tell Us the Complete Story!". *ACS Energy Lett.* **2018**, *3* (3), 622–623.
- (28) Liu, H.; Chen, Z.; Jin, Z.; Su, Y.; Wang, Y. A Reduced Graphene Oxide Supported Cu₃ SnS₄ Composite as an Efficient Visible-Light Photocatalyst. *Dalt. Trans.* **2014**, *43* (20), 7491–7498.
- (29) Lin, X.; Kavalakkatt, J.; Ennaoui, A.; Lux-Steiner, M. C. Cu₂ZnSn(S, Se)₄ Thin Film Absorbers Based on ZnS, SnS and Cu₃SnS₄ Nanoparticle Inks: Enhanced Solar Cells Performance by Using a Two-Step Annealing Process. *Sol. Energy Mater. Sol. Cells* **2015**, *132*, 221–229.
- (30) Zhao, B.; Li, S.; Che, M.; Zhu, L. Synthesis of Cu₃SnS₄ nanoparticles with a Novel Structure as Low-Cost Counter Electrode in Dye-Sensitized Solar Cell. *Int. J. Electrochem. Sci.* **2016**, *11* (8), 6514–6522.
- (31) M, T.; Sharma, N.; Das, T.; Varhade, S.; Badadhe, S. S.; Thotiyl, M. O.; Kabir, M.; Ogale, S. A Combined Experimental and Computational Study of Gas Sensing by Cu₃SnS₄ Nanoparticulate Film: High Selectivity, Stability, and Reversibility for Room Temperature H₂S Sensing. *Adv. Mater. Interfaces* 2018, 5 (10), 1701492–1701500.

- (32) Grimme, S.; Antony, J.; Ehrlich, S.; Krieg, H. A Consistent and Accurate Ab Initio Parametrization of Density Functional Dispersion Correction (DFT-D) for the 94 Elements H-Pu. *J. Chem. Phys.* **2010**, *132* (15), 154104.
- (33) Grimme, S. Accurate Description of van Der Waals Complexes by Density Functional Theory Including Empirical Corrections. *J. Comput. Chem.* **2004**, *25* (12), 1463–1473.
- (34) Xiong, Y.; Xie, Y.; Du, G.; Su, H. From 2D Framework to Quasi-1D Nanomaterial: Preparation, Characterization, and Formation Mechanism of Cu₃SnS₄ Nanorods. *Inorg. Chem.* **2002**, *41* (11), 2953–2959.
- (35) Lin, X.; Steigert, A.; Lux-Steiner, M. C.; Ennaoui, A. One-Step Solution-Based Synthesis and Characterization of Kuramite Cu₃SnS₄ Nanocrystals. *RSC Adv.* **2012**, *2* (26), 9798.
- (36) Narongrit, T.; Somchai, T.; Titipun, T. Characterization of Cu₃SnS₄ Nanoparticles and Nanostructured Flowers Synthesized by a Microwave-Refluxing Method. *Jpn. J. Appl. Phys.* **2013**, *52* (11R), 111201–111205.
- (37) Blaha, P.; Schwarz, K.; Madsen, G. K. H.; Kvasnicka, D.; Luitz, J. {WIEN2K}, {A}n {A}ugmented {P}lane {W}ave + {L}ocal {O}rbitals {P}rogram for {C}alculating {C}rystal {P}roperties; {K}arlheinz Schwarz, Techn. Universität Wien, Austria, 2001.
- (38) Slamet; Nasution, H. W.; Purnama, E.; Kosela, S.; Gunlazuardi, J. Photocatalytic Reduction of CO₂ on Copper-Doped Titania Catalysts Prepared by Improved-Impregnation Method. *Catal. Commun.* **2005**, *6* (5), 313–319.
- (39) Litter, M. I. Heterogeneous Photocatalysis: Transition Metal Ions in Photocatalytic Systems. *Appl. Catal. B Environ.* **1999**, *23* (2–3), 89–114.
- (40) Neatu, Stefan; Maciá-Agullò, J. A.; Concepciòn, P.; Garcia, H. Gold-Copper Nanoalloys Supported on TiO₂ as Photocatalysts for CO₂ Reduction by Water. *J. Am. Chem. Soc.* **2014**,

- 136 (45), 15969–15976.
- (41) Zhu, S.; Liang, S.; Bi, J.; Liu, M.; Zhou, L.; Wu, L.; Wang, X. Photocatalytic Reduction of CO₂ with H₂O to CH₄ over Ultrathin SnNb₂O₆ 2D Nanosheets under Visible Light Irradiation. *Green Chem.* **2016**, *18* (5), 1355–1363.
- (42) Wang, Y.; Zhao, J.; Wang, T.; Li, Y.; Li, X.; Yin, J.; Wang, C. CO₂ Photoreduction with H₂O Vapor on Highly Dispersed CeO₂/TiO₂ Catalysts: Surface Species and Their Reactivity. *J. Catal.* **2016**, *337*, 293–302.
- (43) Zhao, H.; Liu, L.; Andino, J. M.; Li, Y. Bicrystalline TiO₂ with Controllable Anatase-Brookite Phase Content for Enhanced CO₂ Photoreduction to Fuels. *J. Mater. Chem. A* **2013**, *I* (28), 8209–8216.
- (44) Albrecht, P. M.; Jiang, D. E.; Mullins, D. R. CO₂ Adsorption as a Flat-Lying, Tridentate Carbonate on CeO₂(100). *J. Phys. Chem. C* **2014**, *118* (17), 9042–9050.
- (45) Liu, L.; Zhao, C.; Miller, J. T.; Li, Y. Mechanistic Study of CO₂ Photoreduction with H₂O on Cu/TiO₂ Nanocomposites by in Situ x-Ray Absorption and Infrared Spectroscopies. *J. Phys. Chem. C* **2017**, *121* (1), 490–499.
- (46) Liu, D.; Fernández, Y.; Ola, O.; MacKintosh, S.; Maroto-Valer, M.; Parlett, C. M. A.; Lee, A. F.; Wu, J. C. S. On the Impact of Cu Dispersion on CO₂ Photoreduction over Cu/TiO₂. Catal. Commun. 2012, 25, 78–82.
- (47) Di, T.; Zhu, B.; Cheng, B.; Yu, J.; Xu, J. A Direct Z-Scheme g-C₃N₄/SnS₂ Photocatalyst with Superior Visible-Light CO₂ Reduction Performance. *J. Catal.* **2017**, *352*, 532–541.
- (48) Wang, J.; Li, G.; Li, Z.; Tang, C.; Feng, Z.; An, H.; Liu, H.; Liu, T.; Li, C. A Highly Selective and Stable ZnO-ZrO₂ Solid Solution Catalyst for CO₂ Hydrogenation to Methanol. *Sci. Adv.* **2017**, *3* (10), e1701290–e1701300.

- (49) Wang, G. W.; Hattori, H. Reaction of Adsorbed Carbon Monoxide with Hydrogen on Magnesium Oxide. *J. Chem. Soc. Faraday Trans. 1 Phys. Chem. Condens. Phases* **1984**, 80 (5), 1039–1047.
- (50) Teramura, K.; Tanaka, T.; Ishikawa, H.; Kohno, Y.; Funabiki, T. Photocatalytic Reduction of CO₂ to CO in the Presence of H₂ or CH₄ as a Reductant over MgO. *J. Phys. Chem. B* **2004**, *108* (1), 346–354.
- (51) Ji, Y.; Luo, Y. Theoretical Study on the Mechanism of Photoreduction of CO₂ to CH₄ on the Anatase TiO₂(101) Surface. *ACS Catal.* **2016**, *6* (3), 2018–2025.
- (52) He, H.; Zapol, P.; Curtiss, L. A. Computational Screening of Dopants for Photocatalytic Two-Electron Reduction of CO₂ on Anatase (101) Surfaces. *Energy Environ. Sci.* 2012, 5 (3), 6196–6205.
- (53) An, X.; Li, K.; Tang, J. Cu₂O/Reduced Graphene Oxide Composites for the Photocatalytic Conversion of CO₂. *ChemSusChem* **2014**, 7 (4), 1086–1093.
- (54) Kuehnel, M. F.; Orchard, K. L.; Dalle, K. E.; Reisner, E. Selective Photocatalytic CO₂ Reduction in Water through Anchoring of a Molecular Ni Catalyst on CdS Nanocrystals. *J. Am. Chem. Soc.* 2017, *139* (21), 7217–7223.
- (55) Jin, J.; Yu, J.; Guo, D.; Cui, C.; Ho, W. A Hierarchical Z-Scheme CdS-WO₃ Photocatalyst with Enhanced CO₂ Reduction Activity. *Small* **2015**, *11* (39), 5262–5271.
- (56) Kanemoto, M.; Ishihara, K.; Wada, Y.; Sakata, T.; Mori, H.; Yanagida, S. Visible-Light Induced Effective Photoreduction of CO₂ to CO Catalyzed by Colloidal CdS Microcrystallites. *Chemistry Letters*. 1992, pp 835–836.
- (57) Zhang, Y. J.; Sethuraman, V.; Michalsky, R.; Peterson, A. A. Competition between CO₂ Reduction and H2 Evolution on Transition-Metal Electrocatalysts. *ACS Catal.* **2014**, *4* (10),

3742-3748.

(58) Wu, J.; Huang, Y.; Ye, W.; Li, Y. CO₂ Reduction: From the Electrochemical to Photochemical Approach. *Adv. Sci.* **2017**, *4* (11), 1–29.

Figures

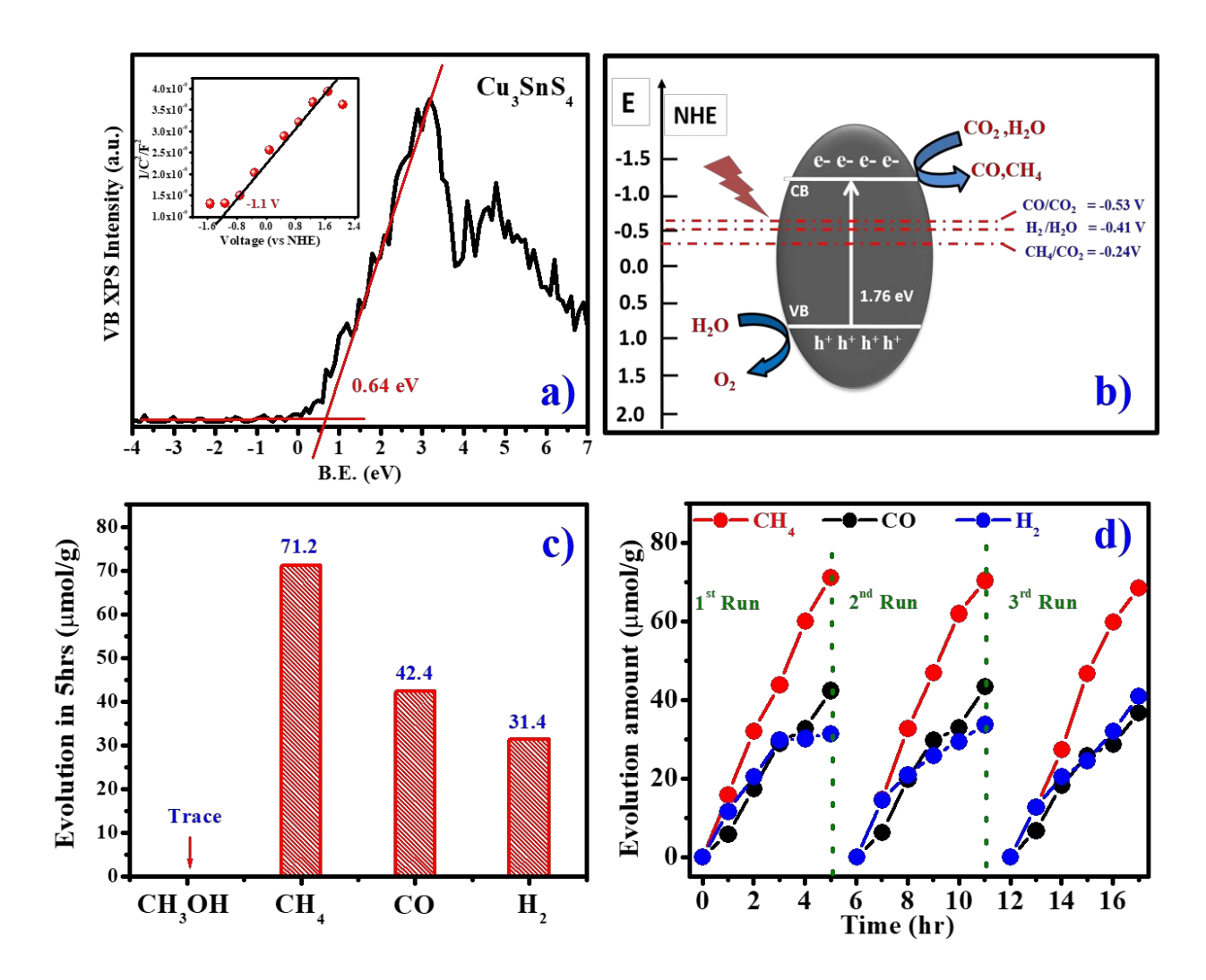


Figure 1. a) Valence Band spectra with Mott Schottky plot in inset. **b)** Energy level diagram. **c)** Evolved reduced products after photocatalytic CO₂ reduction over CTS sample. **d)** Stability profile of CTS.

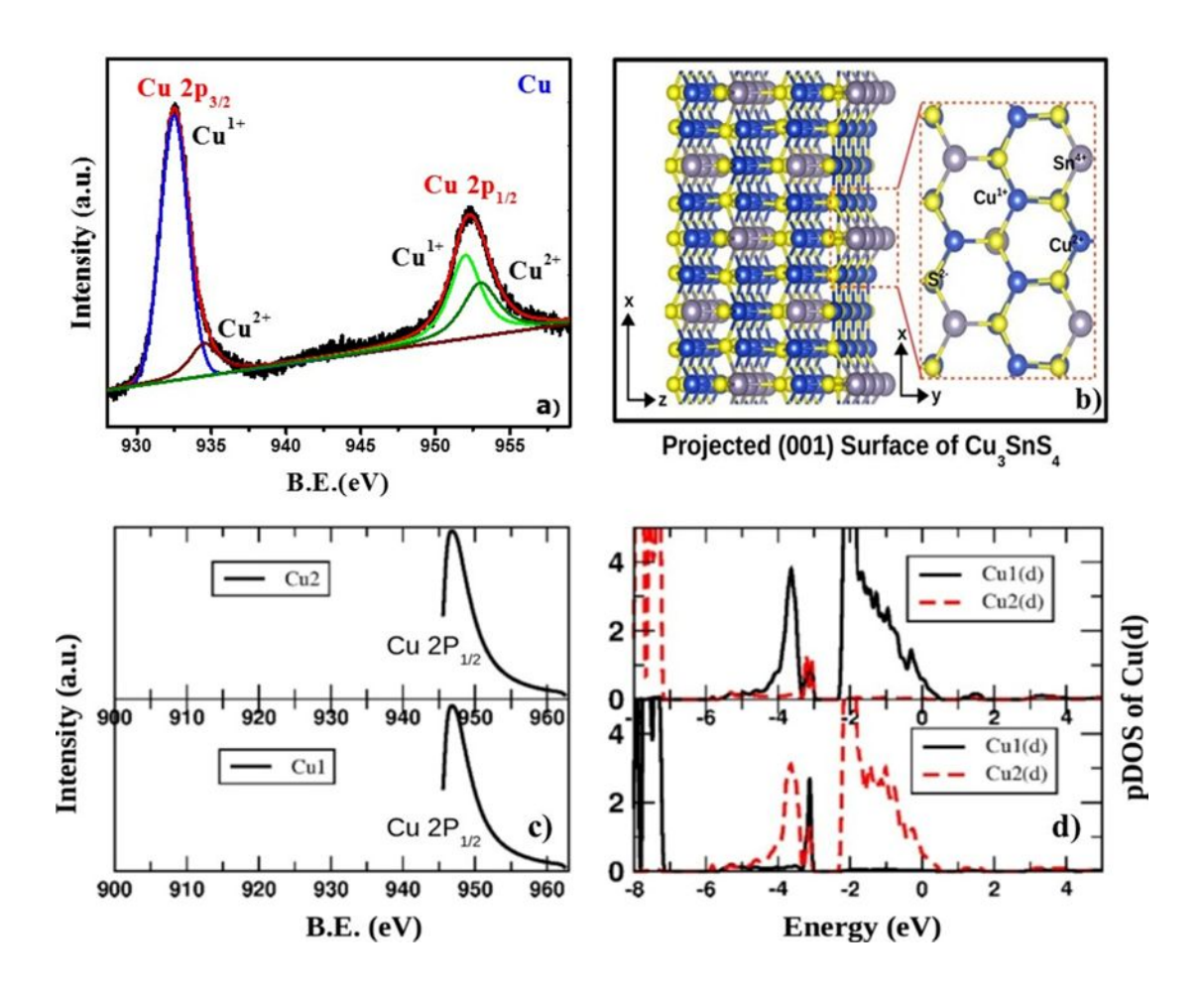


Figure 2. a) XPS spectra of Copper (Cu) over CTS surface. **b)** The optimized four layers slab of CTS grown along <001> which is projected with top most layer exposed upward, with grey balls for Sn, Blue for Cu and yellow for S atoms **c)** The calculated L₂ edges of Cu¹⁺ and Cu²⁺ **d)** Projected density of states (p DOS) from Cu-d of the same Cu1 and Cu2 atoms.

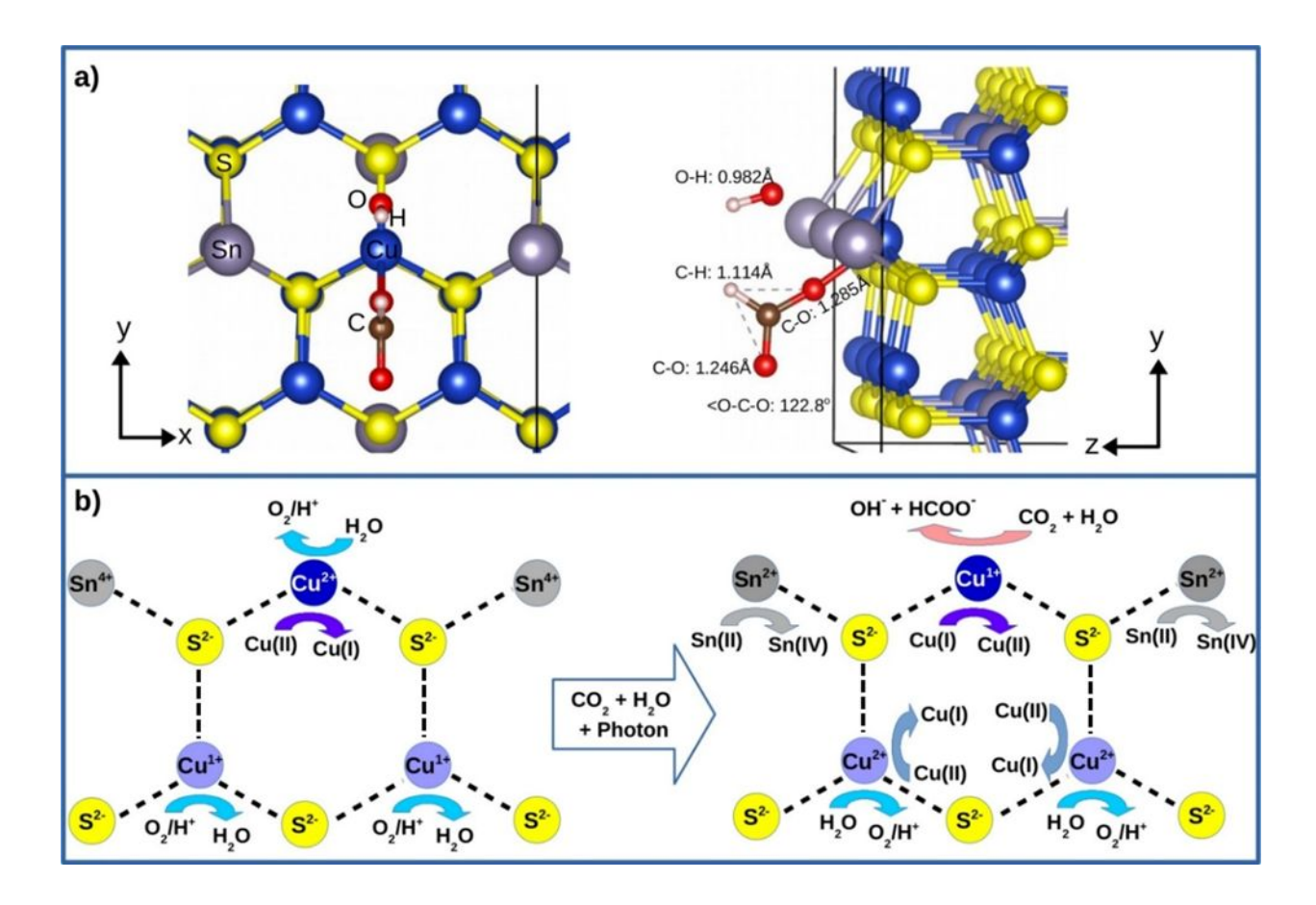


Figure 3. In panel **a**), the optimized geometry of the CTS NPs (001) surface with Cu-Sn termination is exposed to the best-suited CO₂ and H₂O gases and possible formation of formate is shown. In panel **b**), the schematic representation of the CO₂ activation via valence state change of cations of CTS (001) surface viable for the formate route.

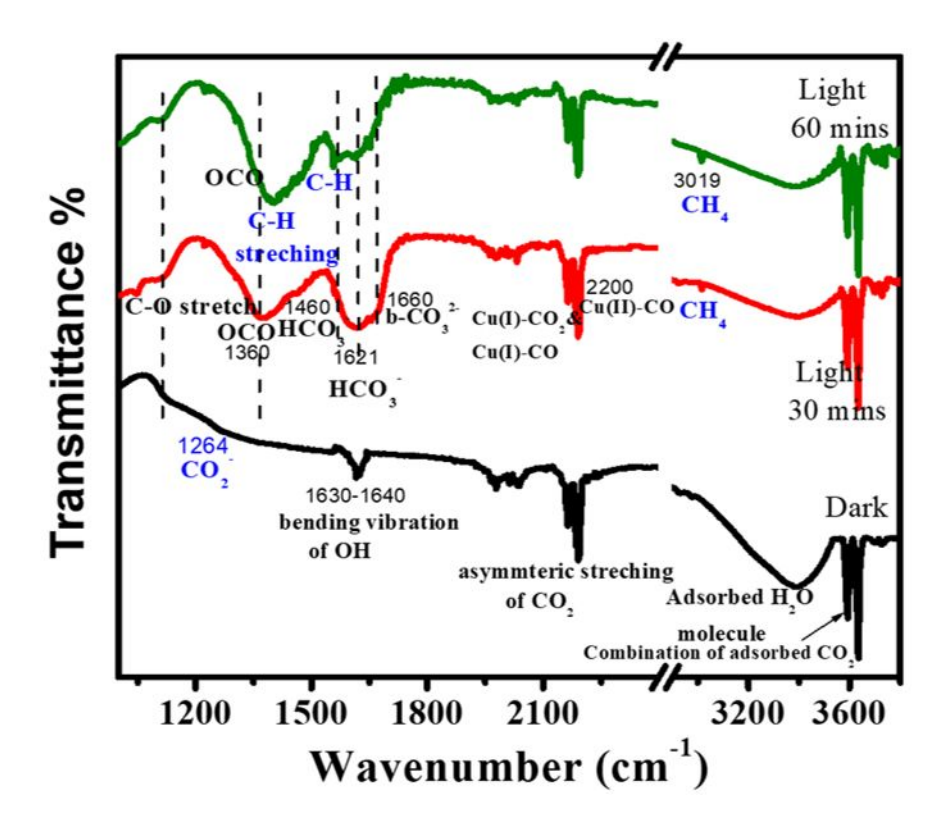


Figure 4. *In situ* Attenuated Total Reflection (ATR) of CTS in presence of purged CO₂ and water vapour.

TOC ENTRY

Experimental and theoretical investigation of Cu-Sn terminated surface of Cu_3SnS_4 for selective photocatalytic CO_2 reduction to CH_4 .

TOC GRAPHIC

